SERI/STR-211-2967
UC Category: 63
DE86010729

MASTER

Photochemical Vapor Deposition of Amorphous Silicon Photovoltaic Devices

Semiannual Subcontract Report
1 May 1985 - 31 October 1985

B. N. Baron
R. E. Rocheleau
S. S. Hegedus
Institute of Energy Conversion
University of Delaware
Newark, Delaware

SERI/STR--211-2967

DE86 010729

June 1986

SERI Technical Monitor:
B. Stafford

Prepared under Subcontract No. XB-4-04061-1

Solar Energy Research Institute
A Division of Midwest Research Institute

1617 Cole Boulevard
Golden, Colorado 80401-3393

Prepared for the
U.S. Department of Energy
Contract No. DE-AC02-83CH10093

TABLE OF CONTENTS

PREFACE

This report describes the first six months of research directed to studies of photochemical vapor deposition for fabricating amorphous silicon based thin-film solar cells. The University of Delaware invested significant resources in the laboratory facilities and equipment needed to perform the research. The interest and support shown by the Solar Energy Research Institute, Solar Electric Division deserve special recognition. Collaboration between this program and work being carried out under SERI Subcontract XL-5-04074-3 has proven to be invaluable.

The following personnel at the Institute of Energy Conversion have contributed to the work described in this report:

Program Manager	B. N. Baron
Principal Investigator	R. E. Rocheleau
Reactor Design/Construction	S. C. Jackson W. A. Buchanan P. Wilson R. Dozier S. Beard
Film Deposition	W. A. Buchanan
Material Characterization	S. S. Hegedus A. R. Moore R. Dozier G. Streetman
Device Fabrication	L. C. DiNetta J. A. Hall A. Canedo
Device Analysis	S. S. Hegedus S. Buchanan

SUMMARY

Objective:

The objective of this research program is to fabricate efficient, stable, single junction amorphous silicon:hydrogen p-i-n solar cells by ultraviolet photo-dissociation of disilane at growth rates exceeding 0.1nm/sec. The primary goal of the research is to fabricate 7% p-i-n solar cells by photo-CVD.

Discussion:

Mercury-sensitized UV photolysis of disilane was selected for depositing a-Si:H films for materials characterization and device development. Several reactor designs were evaluated with primary emphasis on avoiding window fouling. A novel reactor was designed and constructed. The reactor includes a UV transparent moveable Teflon curtain to minimize deposition on the reactor window. UV light is provided by a low pressure mercury grid lamp. Design and construction of the reactor system includes provision for safe handling of toxic and flammable gases. Depositions of undoped a-Si:H were carried out over a range of deposition conditions: reactant gas, 10-30% Si_2H_6 diluted in He; flow rates, 10-20 sccm; reactor pressure, 10-15 torr; mercury partial pressure, 0.012-0.034 torr; substrate temperature, 200-280°C. Undoped films, 490-550 nm thick, were deposited at 0.06-0.07 nm/sec on a variety of substrates for characterization of electrical and optical properties. A systematic study of the influence of substrate temperatures yielded intrinsic a-Si:H films deposited at 240°C having bandgap = 1.85 eV, $\sigma_p = 2.5 \times 10^{-5}$ S/cm, $\sigma_p/\sigma_d = 2 \times 10^5$ and $E_a = 0.64$eV.

Doped, n- and p-type, a-Si:H films were deposited by Hg-sensitized photolysis of Si_2H_6. P-type films with $E_a = 0.4$eV were obtained by adding 0.5-3.0 vol % B_2H_6 to the reactant gas. N-type films with $E_a = 0.25$eV were obtained by adding 1-2 vol % PH_3.

Devices with the configuration glass/TCO/p-i-n/Al were fabricated using photo-CVD deposited a-Si:H layers of 15, 280, and 50nm for the p, i, and n-layers respectively. Current-voltage behavior of the 6 stable unshorted cells under 87.5 mW/cm^2 ELH illumination following a 1 hour heat treatment was: V_{oc} = 0.74 - 0.77V; J_{sc} = 7.7 to 8.7 mA/cm^2; FF = 65.2 to 65.6; and efficiency = 4.5 to 5.1%. The series resistances, measured by dV/dJ at V_{oc}, were 7.0 to 8.1 Ω-cm^2. The spectral response showed peak collection efficiency of 64% at 550 nm. Collection efficiency at 400nm was 24% and 15% at 700 nm and was unaffected by light bias. The spectral dependence of the ratio of collection efficiency as a function of voltage bias indicates that bulk recombination losses were not a significant factor in determining short circuit

current. Open circuit voltages may be limited by insufficient doping of the p- and n-layers.

Future work will include optimizing n-layer conductivity, development of p-type a-SiC, optimizing i-layer thickness and properties, enhanced i-layer deposition rate and characterization of photo-CVD reactor kinetics.

Conclusions:

- A novel photo-CVD reactor which minimizes window fouling was designed and constructed.
- Intrinsic a-Si:H films were deposited and characterized.
- Doped, n-type and p-type, a-Si:H films were deposited and characterized.
- A glass/TCO/p-i-n/metal photovoltaic cell with 5.1% efficiency (87.5 mW/cm^2,ELH) was fabricated by photo-CVD.

SECTION 1.0

INTRODUCTION

Chemical vapor deposition techniques, in particular plasma enhanced CVD, have been used to produce high efficiency a-Si:H p-i-n devices. Several research groups have reported devices with over 10% efficiencies using the plasma enhanced CVD technique. Further development of a-Si:H devices to the point where they will make a contribution to U.S. electrical energy production requires additional research directed to increased efficiency, improved photo-stability, and translation of scale to commercial production.

Research on alternate deposition techniques(1) is likely to lead to improved understanding of the relationships between deposition processes and material properties. Technical options for achieving the properties needed for higher efficiency and long term stability can be expected from such research. Furthermore, understanding of the fundamental chemical processes which govern film growth are required for efficient translation of scale.

A relatively new technique for depositing a-Si:H is photo-CVD. Photo-CVD utilizes ultraviolet light to initiate decomposition of silane or disilane. There are several reports of photo-CVD of a-Si:H. These include direct photolysis at 185nm using disilane (2), and mercury sensitized photolysis at 254nm from silane (3) and disilane (4,5). Recently, a 10.5% efficiency a-Si:H p-i-n photovoltaic cell, fabricated by photo-CVD, was reported (6).

The best reported results from both material properties and device efficiency points of view have been achieved using mercury sensitized photo-CVD. A major limitation in photo-CVD has been preventing deposition on the UV transparent window. Nevertheless, photo-CVD is the best alternative deposition technique for preparing high quality intrinsic and doped materials, for fabricating devices and for studying fundamental materials/preparation relationships.

The research described in this report has as its objective fabrication of efficient, stable, single-junction a-Si:H p-i-n solar cells by mercury sensitized photo-CVD of disilane at growth rates exceeding 0.1nm/sec. The primary goal of the research is fabrication of 7% efficiency p-i-n solar cells by photo-CVD. The research is being carried out under two integrated tasks: material preparation and analysis; and device fabrication and analysis. In this report we describe a novel photo-CVD reactor which minimizes window fouling. Depositions and characterization of device quality intrinsic and doped a-Si:H layers are also described. Finally, the fabrication and preliminary analysis of p-i-n solar cells fabricated by photo-CVD is reported.

SECTION 2.0
MATERIAL PREPARATION AND ANALYSIS

Intrinsic and doped (both n- and p-type) hydrogenated amorphous silicon films were grown by ultraviolet mercury sensitized photo-CVD disilane. While several reactor designs were considered, a novel reactor utilizing a UV transparent moveable Teflon curtain to minimize deposition on the reactor window was designed and constructed. Details of the reactor design, a summary of the film deposition conditions, and characterization of the materials deposited follow.

2.1 EVALUATION OF REACTOR DESIGNS

The photochemical vapor deposition of a-Si is initiated by transmission of UV radiation through a window which forms the top of the deposition chamber. During deposition, the window is subject to becoming coated with deposited material. This coating diminishes the transparency of the window, which diminishes the amount of radiation entering the deposition chamber, thus slowing the rate of deposition and limiting the ultimate thickness of deposition.

Several solutions to the problem of deposition on the window have been proposed. Inoue et al.(4) coated the window with a low vapor pressure oil to prevent deposition of amorphous silicon film on the window. Delahoy(5) and Konagai(6) have also used low vapor pressure oil on the window. T. Kazahaya(7) used a stream of nitrogen gas near the window similar to the approach described by D. D. Allred et al.(8). Finally, J. W. Peters and F. L. Gebhart(9) described photochemical vapor deposition of silicon nitride passivation layers in a reactor utilizing a transparent polyvinylidene fluoride film across the internal face of the window within the reaction chamber. Movement of the film across the window is provided to remove material deposited on the film from the path of incoming radiation and to prevent deposition on the window. Guide rolls were provided for optimal spacing, including contact, between the mobile film and window.

None of these solutions have proven to be entirely satisfactory. Coating the reactor window with oil may introduce contamination and is not effective for long periods of time as would be required in a production facility. Providing a stream of non-reactive gas across the face of the reactor window has limited effectiveness due to unavoidable transport of reactive gases at low pressures to the window especially when larger windows and deposition areas are used. The mobile transparent window of Peters et al.(9) requires a mechanically imposed gas-tight seal between the film and reactor window. Leakage of

reactive gas into the space between the film and window is difficult to avoid during long periods of operation.

For these reasons, a novel two chamber reactor was designed which uses a transparent moveable film to remove deposited film from the path of the incoming radiation but utilizes gas flows and chemistry to minimize diffusion of reactants to the region of the window and to eliminate unwanted deposition on the window.

2.2 PHOTO-CVD SYSTEM AND REACTOR

Equipment from the thermal CVD apparatus used in Phase 1 of this contract and additional expenditures by the university were used to build a laboratory for two photo-CVD reacting systems. The gas handling and gas storage were designed for safety and nigh purity. Key features of the gas manifolds and storage facilities are summarized in Table 1.

A schematic of the photo-CVD reactor is shown in Figure 1, and key components of the reactor are described in Table 2. As shown in the figure, a flexible curtain separates the reactor into two chambers. The curtain is sealed to the walls of the reaction chamber by a weighted plate and by higher pressure in the upper window chamber to minimize diffusion of reactants from the lower to upper chamber.

Inert and/or reaction inhibiting gases are fed into the upper window chamber. These gases can contribute to the reduction or elimination of window fouling in several ways.

° Gases diffusing around the curtain are highly diluted, lowering their partial pressure in the window chamber thus reducing the rate of film growth.

° Gas phase reactions in the upper chamber can be modified by the gases thus inhibiting formation of the gas phase precursors necessary for film growth.

° Surface reactions on the window may be modified to minimize film formation.

Reactant and inert gases are fed into the lower deposition chamber after passing through a mercury bubbler as appropriate.

The reactant and inert diluent gases are distributed through the reaction chamber by a gas distribution manifold within the reactor. Four 1"x1" substrates are mounted on the heated stainless steel pedestal. Figure 2 shows the actual substrate temperature as a function of the measured pedestal temperature. Other operating conditions are described in the sections below for each of the film types.

TABLE 1

Key Features of Gas Storage and Gas Handling System

Safety

- Flow Limiting Valves
  Veriflow Model FLV-120 series
- No Connection Outside Ventilated Area
- Exhaust Gas
  Diluted with N_2 in pump casing
  High temperature decomposition
- Automatic feed gas shutoff interlocked to:
  - loss of ventilation
  - reactor overpressure
  - loss of power
  - fire alarm
  - panic buttons
- Gas Storage
  AIRCO Gas cabinets outfitted with sprinkler heads

Gas Handling and Metering

- 9 Mass flow controllers
  Tylan Model FC-260, FC-360
  Si sources - SiH_4, Si_2H_6
  Ge source - GeH_4
  Dopant - PH_3, B_2H_6
  Diluents - Ar, He, H_2
- Tubing and fittings
  1/4 in OD .035 wall 304 SS
  316 SS CAJON VCR fittings with Ni gaskets
- Dopant isolation - double block valve and vacuum bleed between valves
- Valves
  NUPRO `B' series bellows
  NUPRO 4DS series diaphragm
- Pump
  Leybold Heraeus Model No. D30AC
  Fomblin oil, LVAC 25/5, with continuous filtration
- Purging - deep purge provided before regulator in gas cabinets

TABLE 2

Components of Photo-CVD Reactor

304 SS O-ring sealed body

UV transparent quartz windows 4" x 3/8"

Esco Products, Inc.

304 SS Substrate blocks, accommodates 4-1 inch square substrates

Movable curtain

DuPont "TEFLON" PFA - LP-100

≥90% transmission at 254 nm

Light source

Low pressure Hg vapor lamp

BHK Inc. model 88-9102-02

12-15 mw/cm^2 @ 1 inch

Hg bubbler

25-150°C operating range

25 mm deep pool of Hg

Rotary feed through Varian Model P-253 for curtain movement

FIGURE 1

Schematic of Photo-CVD Reactor

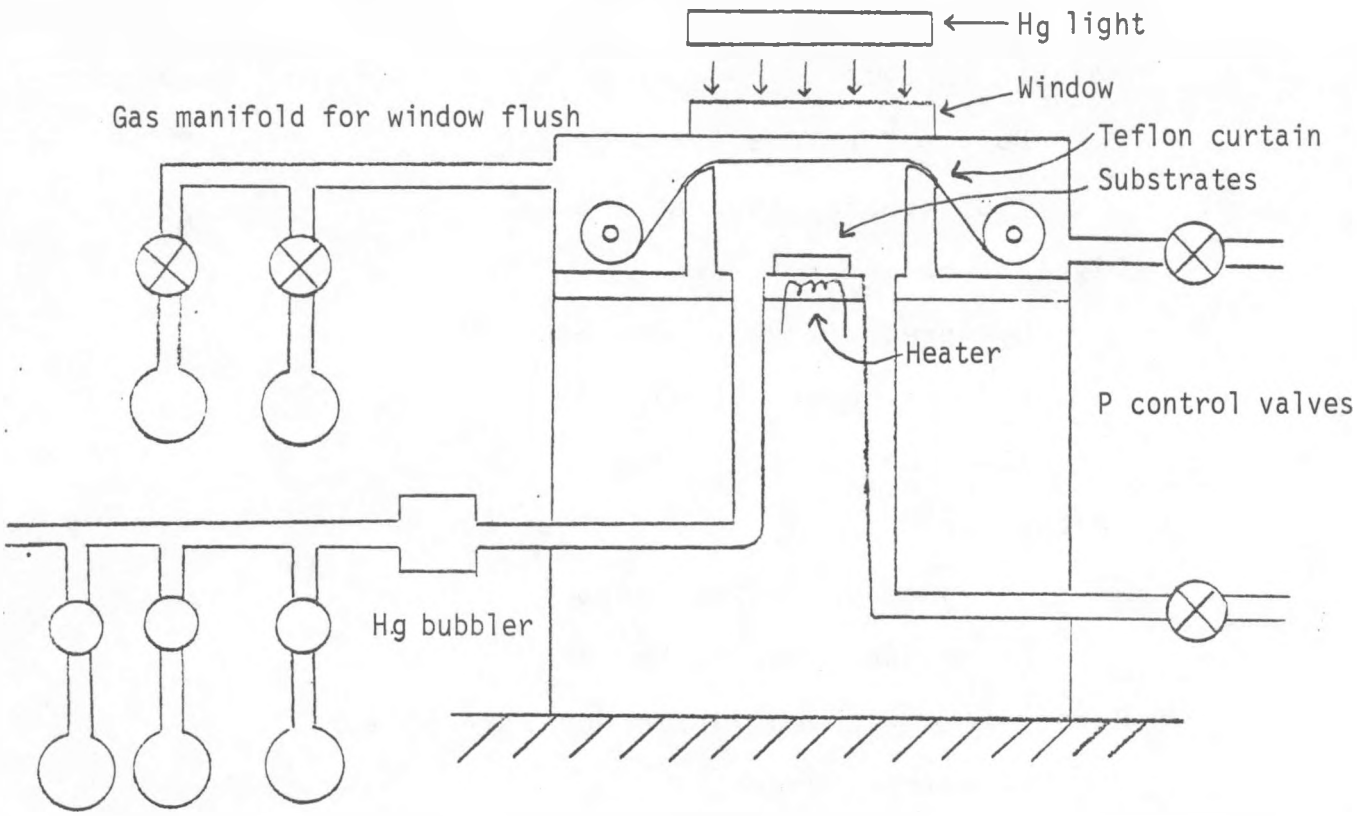

- Si_2H_6
- He
- Ge
- B_2H_6
- PH_3
- Hydrocarbon

FIGURE 2

SUBSTRATE TEMPERATURE CALIBRATION

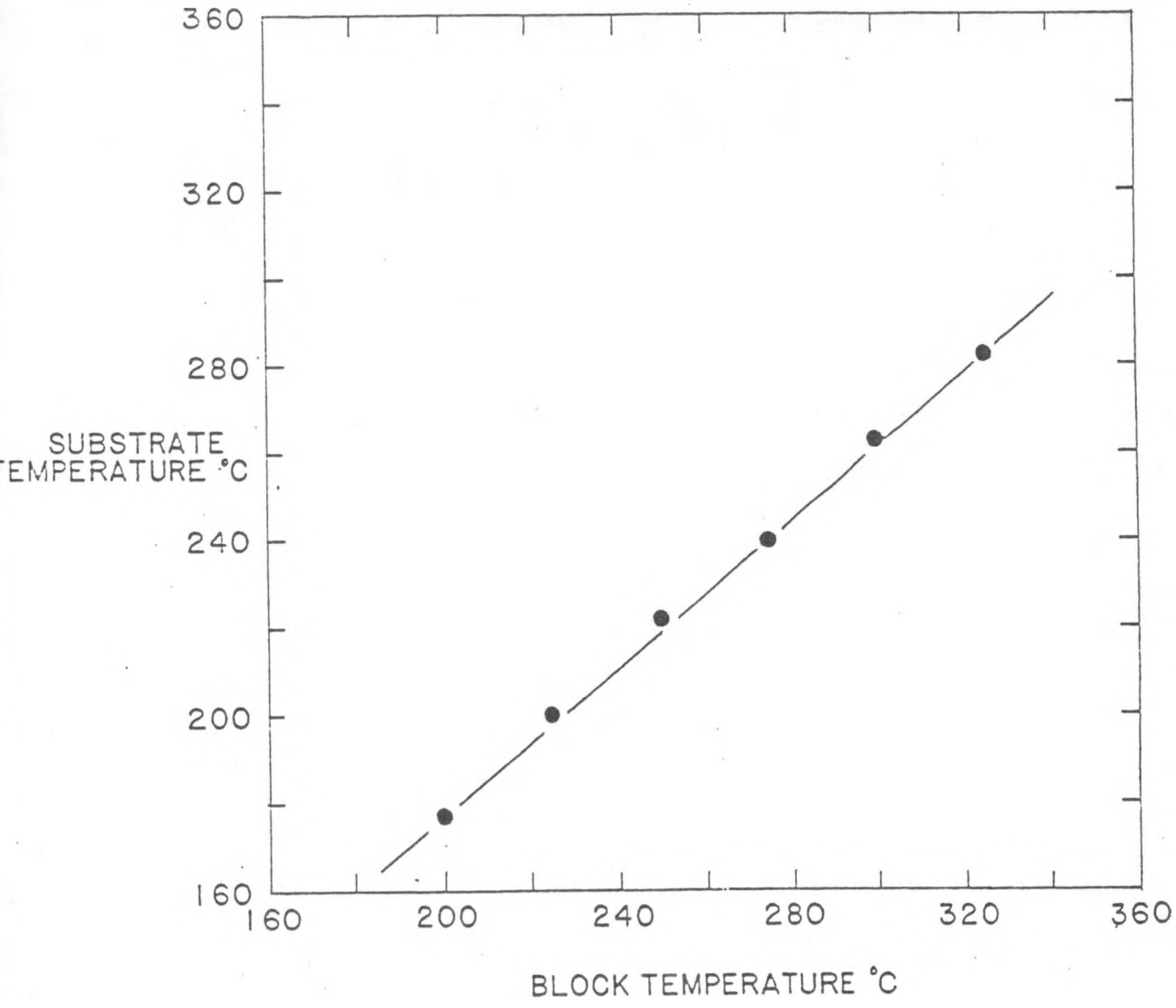

2.3 INTRINSIC FILMS

2.3.1 Deposition/Reactor Characterization:

Intrinsic amorphous silicon films have been deposited under the range of conditions summarized in Table 3. Material properties are described in section 2.3.2.

TABLE 3

Summary of Intrinsic Layer Deposition Conditions

Parameter	Range
Reactor Pressure	10-15 torr
Substrate Temperature	200-280°C
Hg Bubbler Temperature	50-65°C
Disilane Type	Honjo disilane
Flow	1-3 sccm
Mole %	10-30% in He

The initial intrinsic film depositions were used to develop a preliminary reactor model allowing quantitative evaluation of the effects of film growth on the window and Teflon curtain on the rate of deposition and film thickness. Although many simplifying assumptions were made, the use of this model led to process and reactor design changes which have resulted in the growth of intrinsic films over 500nm thick at growth rates around .06 to .07nm/s with no measurable window fouling. A brief description of this model follows.

An estimate of the effect of window fouling, film deposition on the Teflon curtain and the frequency at which the curtain is moved to expose uncoated sections can be calculated assuming that the film growth rate is proportional to the intensity of light. If the intensity and film growth at the surface of an unfouled window are I_o and R_o respectively, and it is assumed that the transmitted light decreases exponentially with the amount of a-Si deposited on the window; then the rate of film growth on the window (dx_o/dt) is described by

$$\frac{dx_0}{dt} = \frac{I_1}{I_0} R_0 = e^{-\alpha x_0} R_0 \qquad (1)$$

where α = the absorption coefficient at the excitation wavelength
I_1 = the light intensity through the window with a film of thickness x_0.

By design, the growth rate on the window side of the curtain is negligible compared to the substrate side. With this constraint, the growth on the substrate side of the curtain (dx_1/dt) is

$$\frac{dx_1}{dt} = \frac{I_2}{I_0} R_1 = \frac{I_2}{I_1}\frac{I_1}{I_0} R_1 = e^{-\alpha(x_0+x_1)} R_1 \qquad (2)$$

where I_2 = the light intensity after passing through the film on the curtain
x_1 = film thickness on the curtain
R_1 = growth rate on the substrate side of the curtain at intensity I_0.

The initial film growth rates at the window and on the curtain, R_0 and R_1 respectively, are different due to the differing gas compositions and reaction rates in the two chambers. If one also makes the simplifying assumption that the film growth rate on the substrates equals that on the curtain then

$$x_2 = \sum_i x_1(i) \qquad (3)$$

where x_2 = film thickness on substrate
$x_1(i)$ = film thickness on curtain during interval i

For the case where there are no deposits on the curtain, window and substrates at the start and where the curtain is moved periodically so that light is transmitted through a clear new section of curtain, the boundary conditions are:

$$x_0 = 0 \ @ \ t = 0 \qquad (4)$$

$$x_1 = 0 \ @ \ t = nt_1 \qquad (5)$$

$$n = 1,2,3,\ldots N-1 \qquad (6)$$

$$x_2 = 0 \ @ \ t = 0 \qquad (7)$$

where

t = elapsed time, seconds

t_1 = exposure time per frame of curtain, seconds/frame

nt_1 = elapsed time when curtain is periodically moved

n = the current frame number less one

N = the total number of frames exposed during a complete run.

Solving equations 1 through 3 with boundary conditions 4 through 7 yields

$$x_0 = \frac{1}{\alpha} \ln(\alpha R_0 t + 1) \tag{8}$$

For $t = nt_1$ to $t = (n+1)\, t_1$

$$x_1 = \frac{1}{\alpha} \ln \left(\frac{R_1}{R_0} \ln\left(1 + \frac{\alpha R_0 t}{\alpha R_0 n t_0 + 1}\right) + 1 \right) \tag{9}$$

The total film thickness on the substrate is

$$x_2 = \sum_{n=0}^{N-1} x_1(n) \tag{10}$$

The average deposition rate at the substrate is found by dividing x_2 by the total run time:

$$\text{Ave. Rate} = x_2/(Nt_0) \tag{11}$$

Equation 8, 9, and 11 have been used to separate the effects of the frequency of curtain travel and window fouling and to guide reactor and process modifications during start-up. Figure 3 shows the calculated average growth rates as a function of curtain exposure time and initial window fouling rate (R_0) for an assumed rate of 1.6 Å/s at the initial intensity(R_1).

The points shown in Figure 3 represent actual operating experience. The points are numbered in chronological order. Refinements in the operation of the reactor are shown as increases in the apparent growth rate. The data shown in Figure 3

FIGURE 3

Apparent Deposition Rate as a Function of Curtain Speed and Window Fouling Rate

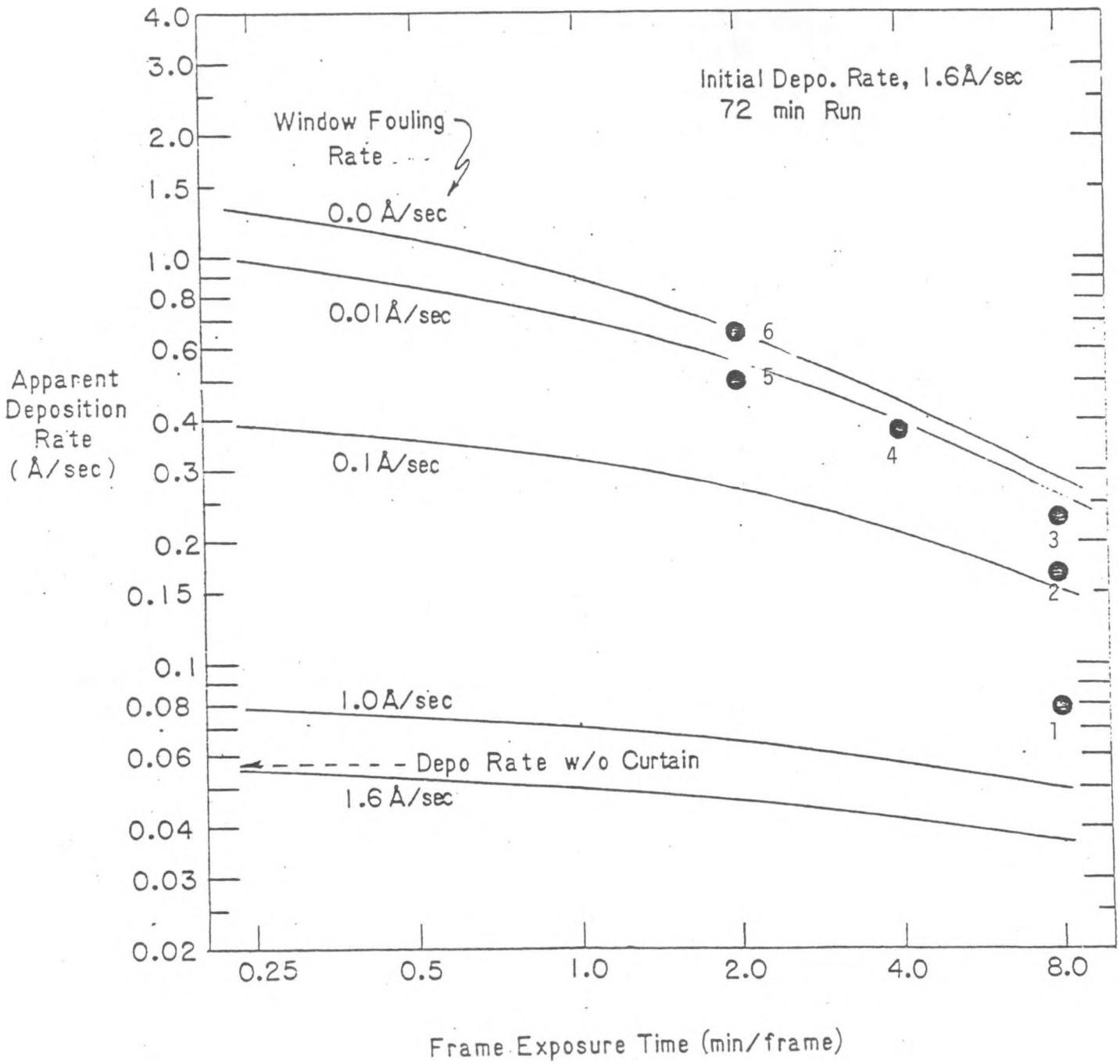

were obtained with a 65°C Hg bubbler, 20% Si_2H_6 in He, and a reactor pressure of 15 torr. Although substrate temperature did vary from 200 to 280°C, subsequent work has shown that the growth rate of undoped a-Si films is independent of temperature. A discussion of the refinements in the reactor operation and interpretation of the resulting increase in the growth rate follows:

From point 1 to 2: The window flush flow rate was increased 50%. This diluted any reactants that may have diffused through or around the curtain, reduced the window fouling rate and consequently allowed more light into the reaction chamber. The ratio of the window transmission at the end of the deposition to the transmission of the clean window (I_{1f}/I_o) increased by a factor of 4.

From point 2 to 3: The mechanical seal was improved. This reduced the diffusion of gases around the curtain and further reduced the window fouling rate. The ratio (I_{1f}/I_o) improved by 40% as a result.

From point 3 to 4: The mechanical seal between the curtain and reaction chamber walls was further improved and the exposure time per frame of curtain was reduced from 8 minutes to 4 minutes. Again the better mechanical seal improved the light intensity ratio, I_{1f}/I_o by ~40%. As a result of the less window fouling and higher curtain usage the average growth rate increased 60%.

Points 4 to 5: The exposure time per frame was reduced from 4 to 2 minutes. Though there was no reduction in the window fouling rate since the conditions in the window flush chamber and sealing were unchanged. The apparent deposition rate increased 30% because of the higher curtain usage in close agreement with the calculations.

Points 5 to 6: Optimization of the window chamber purge gas composition effectively eliminated window fouling.

Following the successful deposition of film without window fouling(point 6, deposition no. 9) a series of depositions were carried out to characterize intrinsic films. As described in detail below, the substrate temperature was varied from 200 to 280°C. Measurements using 254nm UV light showed no change in transmission through the window with the deposition of 400-500nm of a-Si on the substrates at rates from .045 to .07 nm/s.

2.3.2 Film Properties:

Intrinsic layers deposited within the range of conditions summarized in Table 3 have been characterized using:

1. Optical absorption

2. Room temperature dark conductivity and photo-conductivity

3. Dark conductivity as a function of temperature

4. IR absorption spectroscopy

5. Hole diffusion length by surface photo voltage

6. Density of states by space charge limited current (SCLC)

7. Sub-band gap absoprtion from primary photocurrent spectra

Optical gap has been determined using Tauc plots assuming both first surface and multiple reflections as shown in Figure 4 for an i-layer deposited at 240°C. The values of optical gap reported here represent the average of the values obtained with these two assumptions.

Dark conductivity as a function of temperature and photoconductivity at room temperature were measured using i-layers deposited on 2000A thick molybdenum contacts 1 mm apart in a gap cell configuration. Photo-conductivity was measured using ELH light at approximately 100 mW/cm^2. Activation energy was determined from Arrhenius plots of $\sigma_d(T)$ measured between 50 and 200°C.

Figure 5 summarizes the results of these characterizations for films deposited at 200, 220, 240, and 280°C. Also shown in Figure 5 are i-layer film properties reported by Inoue and Konagai(4) deposited at higher flow rates and lower pressures but similar temperatures.

IR absorption spectra measured at SERI on samples deposited at 200 and 280°C on single crystal silicon are shown in Figure 6. The SiH_2 bond-stretching ($2090cm^{-1}$) and bond-bending ($890cm^{-1}$) is evident in the sample deposited at 200°C while the high temperature sample shows only Si-H bonding. The 630 cm^{-1} absorption peak was integrated to estimate the percent of bonded hydrogen (10) yielding 12% and 6% for the samples at 200 and 280°, respectively.

Diffusion length was measured by the constant surface photovoltage method on intrinsic layers deposited on n+/Mo/7059 substrates using n+ by thermal CVD. A value of L_D = .21 μm was obtained with 1 sun red bias light for a .55μm thick i-layer deposited at 280°C as shown in figure 7.

The density of states (DOS) distribution within the band gap was determined by denBoer's step-by-step method(11) from J-V characteristics measured on Ni/i/n+(c-Si) sandwich structures.

The n^+c-Si wafer was As doped with a resistivity of .1Ω-cm. The i-layers were approximately .6μ thick. The DOS distributions are shown in Figure 8 for i-layers deposited at 240° and 280°C after annealing for 1 hour at 150°C in air. The minimum DOS for the sample deposited at 280°C was approximately twice that of the 240°C sample, $3x10^{16}$ and $1.5x10^{16}$ respectively. The position of the minimum (.63eV) agrees well with the activation energies.

FIGURE 4

Summary of Optical Analysis

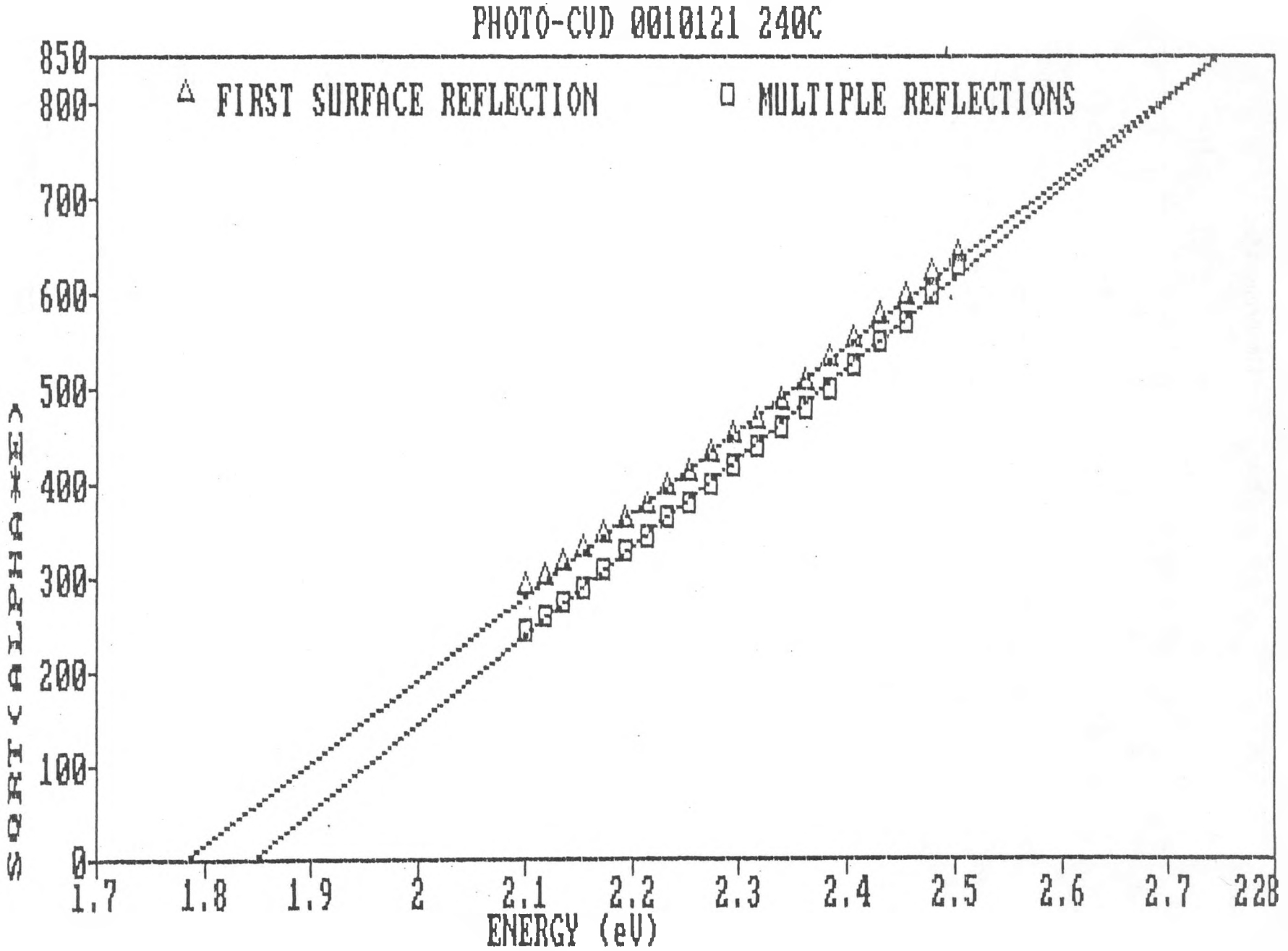

FIGURE 5

Summary of Intrinsic Film Properties

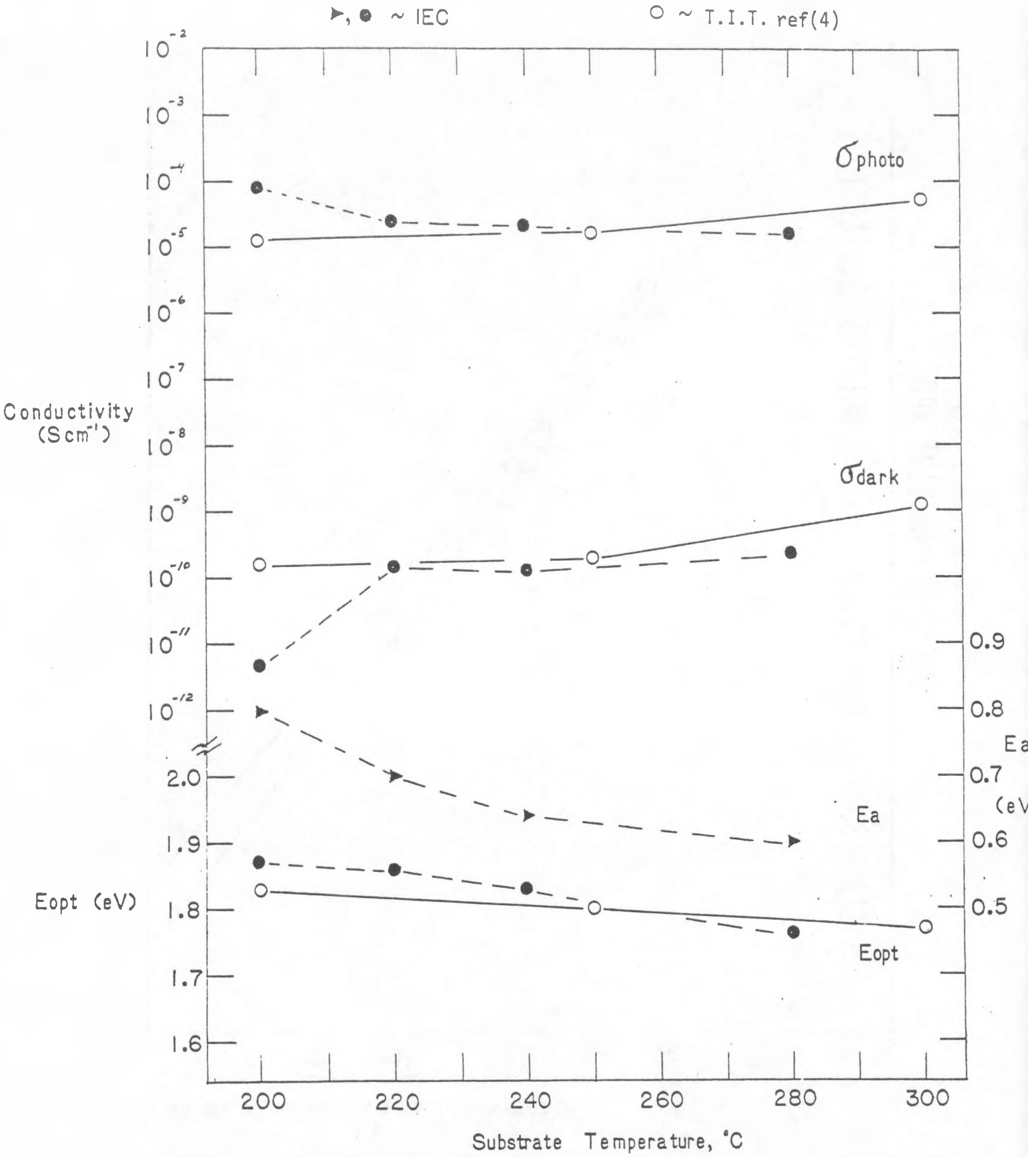

FIGURE 6

IR Absorption Spectra of i-Layers

Deposited at 200°C (top) and 280°C (bottom)

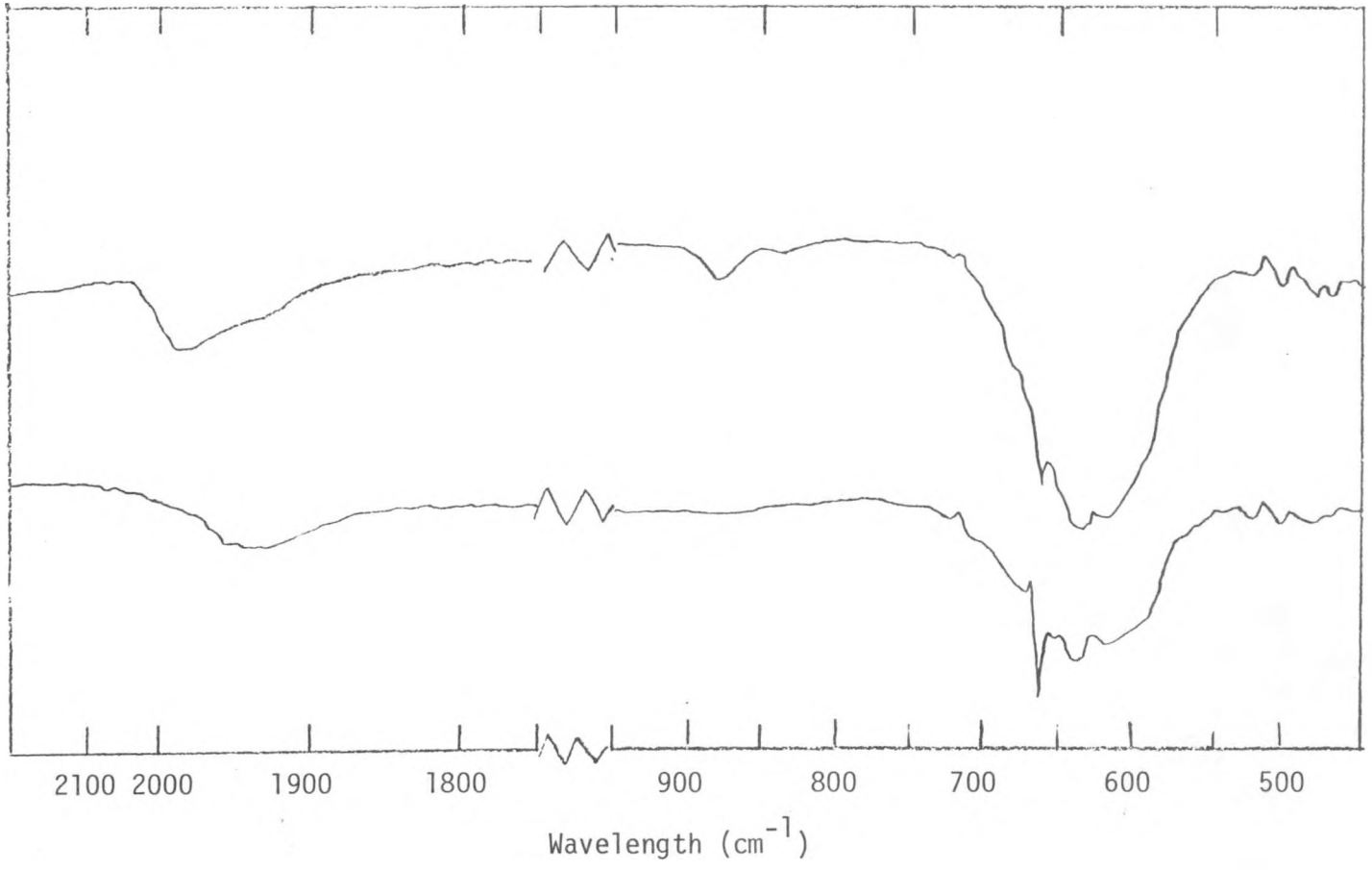

FIGURE 7

DIFFUSION LENGTH BY

SURFACE PHOTOVOLTAGE

SAMPLE NO.:	12.122
SUBSTRATE :	CVDN/Mo
I-LAYER :	20% HONJO DISILANE IN He
	10 sccm
	15 torr
	.034 torr Hg
	280°C
	0.55 MICRONS
DIFFUSION LENGTH:	0.21 MICRONS

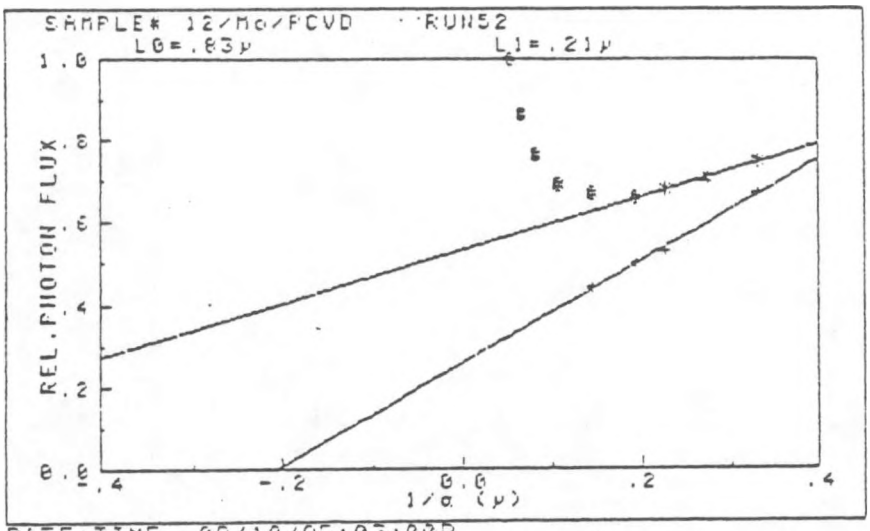

DATE:TIME 09/10/85:03:00P

TAUC COEFFS(Alpha*E FORM): Eg= 1.720 Ev C= 7.965 Microns^-1/2 Ev^-1/2

Vbi=0.53 Volts

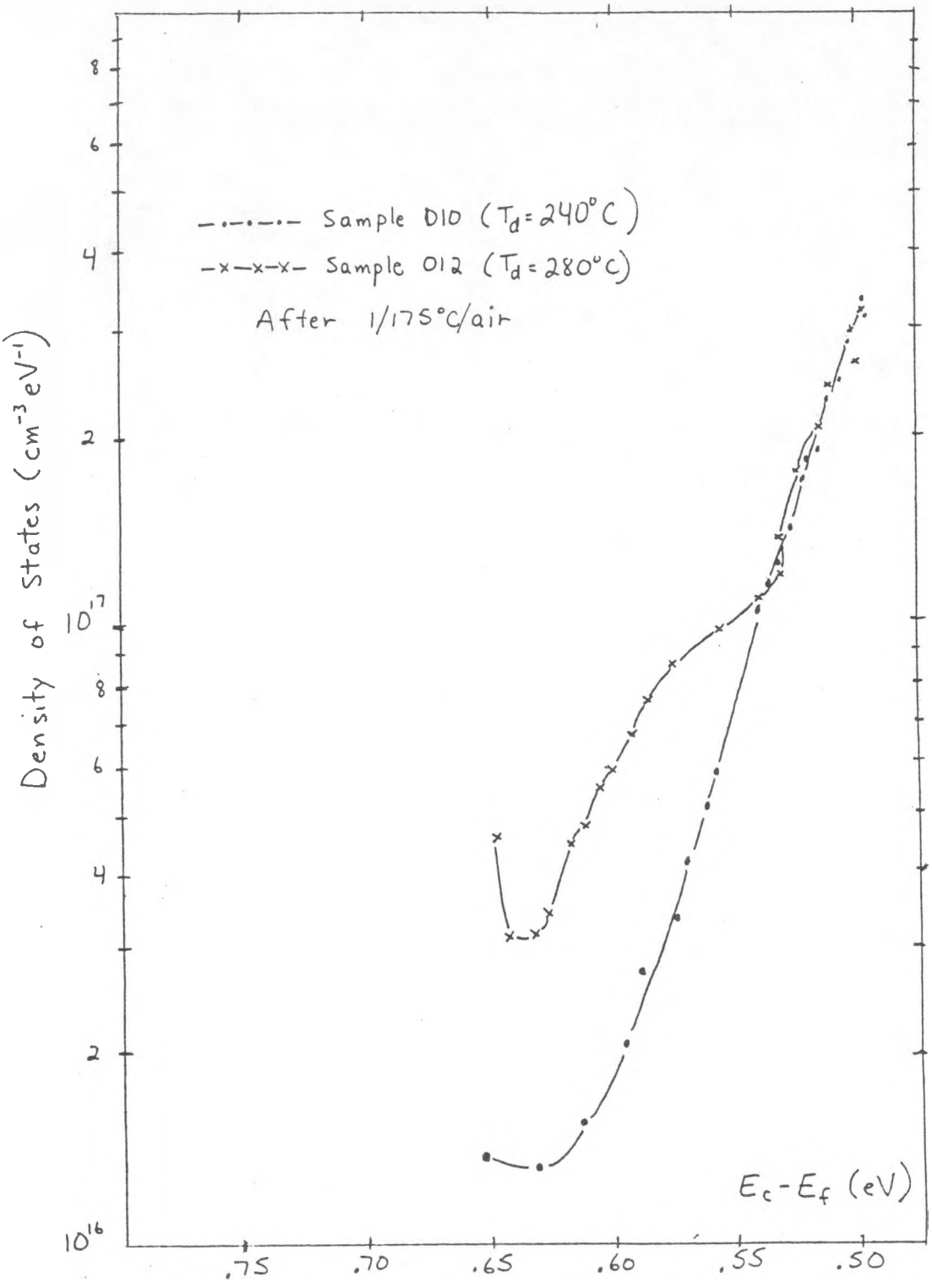

FIGURE 8. Density of States from SCLC of Photo-CVD i-Layers Deposited at 240 and 280°C.

shown in Figure 5. Although these photo-CVD films are less intrinsic than the thermally deposited films (minimum DOS at .63 and .7-.8eV respectively), they have nearly an order of magnitude lower DOS.

The Urbach edge (exponential absorption tail) was determined from the sub-gap primary photocurrent spectra (n_c) shown in Figure 9 on a SnO_x/pin/Al device (see Section 3.1). A value of the characteristic energy E_o of .049 eV was obtained from analysis of the slope of ln (n_c) vs E in the range from 1.45 to 1.60eV.

2.4 p-LAYERS

Boron doped p-type a-Si:H films were deposited using Hg sensitized photo CVD with 7 to 28% Si_2H_6 in He. Films were deposited using 1% B_2H_6 in Argon with B_2H_6/Si_2H_6 ratios of .0016 and .005 at a substrate temperature of 200°C. Attempts to deposit films at higher B_2H_6/Si_2H_6 ratios with this diborane source resulted in large quantities of powder and poor film adherence. Adherent films were deposited and characterized at higher ratios, .015 to .028 using 4.7% B_2H_6 in H_2 as the dopant source.

The growth rate was significantly enhanced by the addition of diborane. With B_2H_6/Si_2H_6 = .015 the average growth rate was 0.12 nm/s at 200°C and 0.17 nm/s at 240°C compared to approximately 0.065 nm/s at similar reaction conditions without diborane.

The optical gap, room temperature dark conductivity and photoconductivity and activation energy of the dark conductivity as a function of B_2H_6/Si_2H_6 ratio are summarized in Figure 10. Devices described in section 3 were made using p-layers grown with a B_2H_6/Si_2H_6 ratio of .013.

2.5 n-LAYERS

Phosphorous doped n-type a-Si:H films were also deposited using Hg-sensitized photo-CVD with 20% Si_2H_6 in He. Films were deposited using 4.3% PH_3 in H_2 with PH_3/Si_2H_6 ratios of .01 and .02 at a substrate temperature of 240°C. Film properties are summarized in Figure 10. In these preliminary experiments, the two-fold increase in PH_3 partial pressure did not significantly change the film properties. Activation energies around 0.25eV with PH_3/Si_2H_6 ratios from .01 to .02 have been achieved. The devices described in section 3 were made using n-layers grown with a PH_3/Si_2H_6 ratio of .015.

It is not possible to evaluate the effect of PH_3 on growth rate at this time due to loss of curtain integrity during these two runs which caused substantial window fouling.

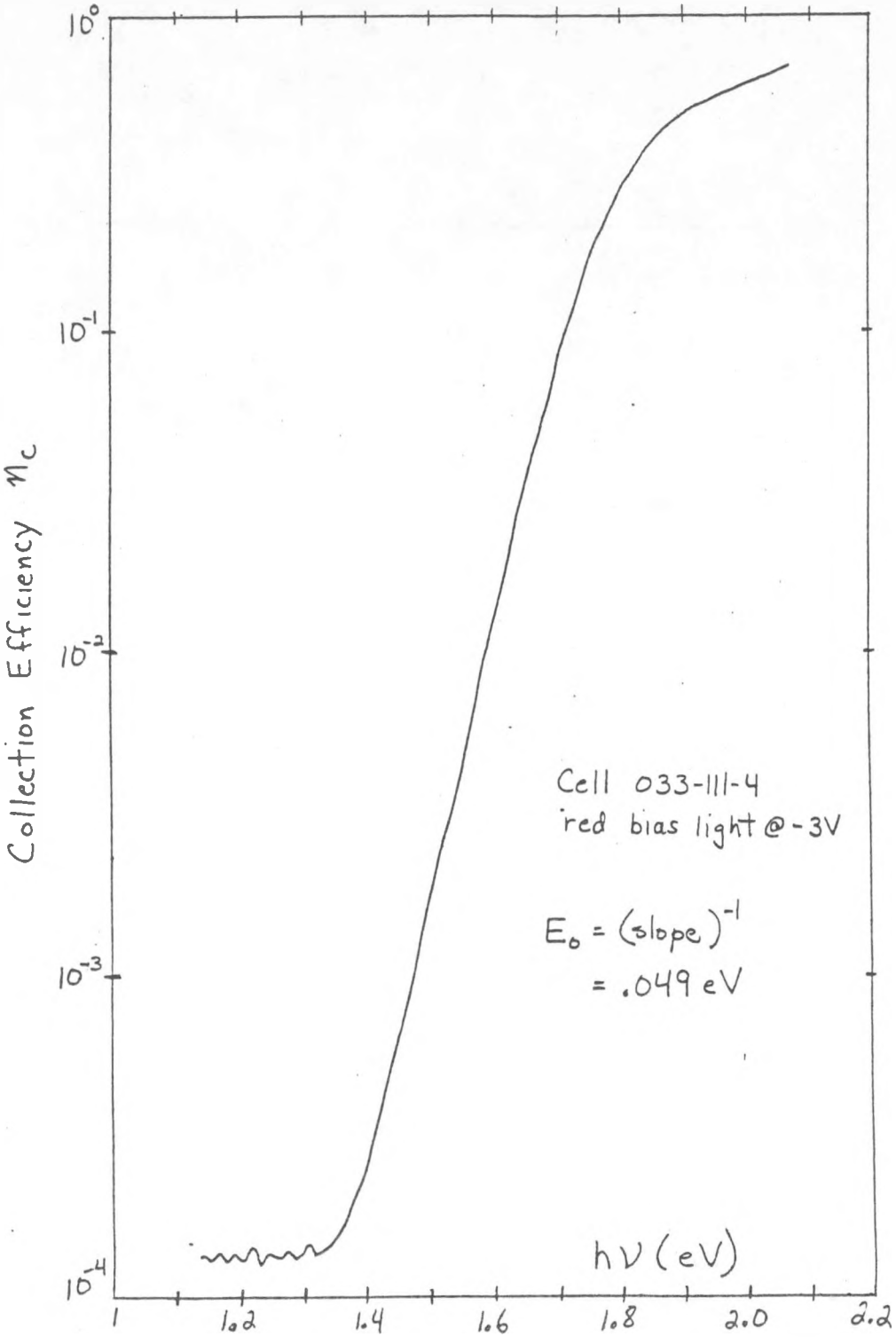

FIGURE 9. Sub-band Gap Collection Efficiency from Primary Photocurrent Measurements

FIGURE 10
Summary of Doped Film Properties

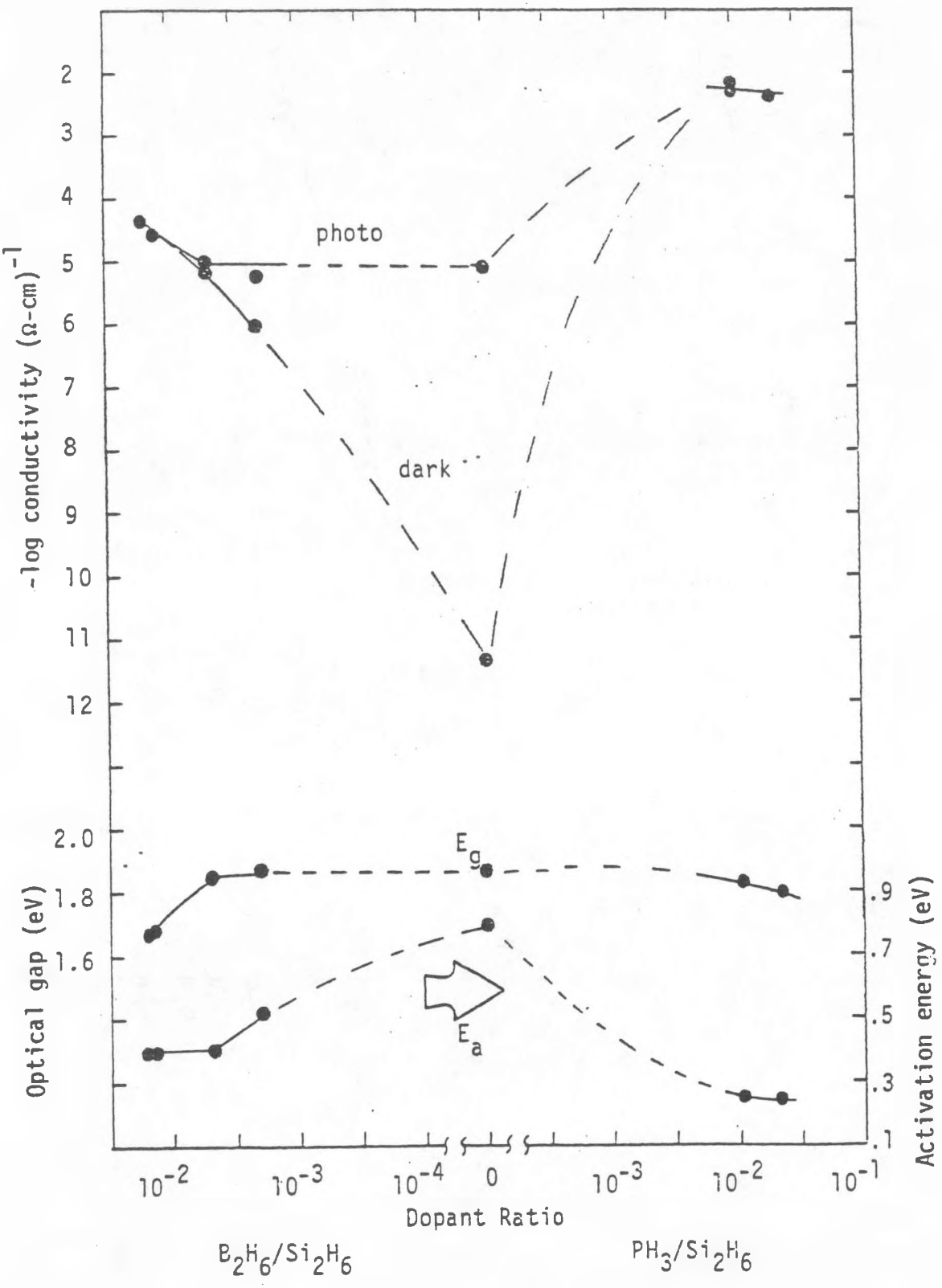

SECTION 3.0

DEVICE FABRICATION AND ANALYSIS

Following preliminary exploration of deposition parameters described in section 2, photo-CVD pin devices were made and characterized. Details of the fabrication and analysis follow.

3.1 DEVICE FABRICATION

Initial test cells (run 33) were fabricated using Cherry Electric SnO_x substrate, photo-CVD deposited p-i-n layers, and e-beam deposited Al for back contact. The substrates were cleaned using a hot detergent wash, deionized H_2O rinse and solvent drying. The semiconductor layers were deposited at the conditions described in Section 2 with the i-layer deposition at 240°C. The p, i, and n-layers were approximately 15, 280, and 50nm thick respectively. The cell fabrication was completed by e-beam evaporation of Al. Twelve 3mmx3mm cells were defined by photolithography and etching of the Al. An initial cell test was made with this configuration. The cells were retested following removal of the a-Si outside the defined cell area by plasma-etching at room temperature.

3.2 DEVICE ANALYSIS

In order to evaluate the effects of the processing steps on device behavior, current-voltage characteristics of the cells on substrate 33-111 were tested in the following sequence: initial test after Al etching; a week later after plasma-etching of the a-Si down to the SnO_x; after a 1 hour 175° air heat treatment; and finally one month later to examine the effect of storage.

Cell results are shown in Appendix A. The J-V curve of cell no. 5 from 33.111 from the 12/18/85 retest is shown in figure 11. At this final test the cell efficiency was 5.13% (at 87.5mW/cm^2,ELH light) with the following characteristics: V_{oc} = .765V, J_{sc} = 9.08 mA/cm^2, FF = 64.6 and dv/dj at V_{oc} = 6.9Ω-cm^2. The most significant changes with heat treatment were improvements in V_{oc} and FF. The diode quality factor after heat treatment was 1.59.

The resistance at V_{oc} (R_{Voc}) was analyzed using the Swartz technique(12). This allows separate determination of defined contact resistance and the photoconductive resistance from the value of R_{Voc}. This analysis for cell 33-111-5 indicates a contact resistance of 1Ω-cm^2 and a photoconductive resistance of 1.4 -cm^2 at 87.5 mW/cm^2.

The spectral response of cell 33-111 with light bias at 0 and -1V and in the dark at 0V is shown in figure 12. The close agreement

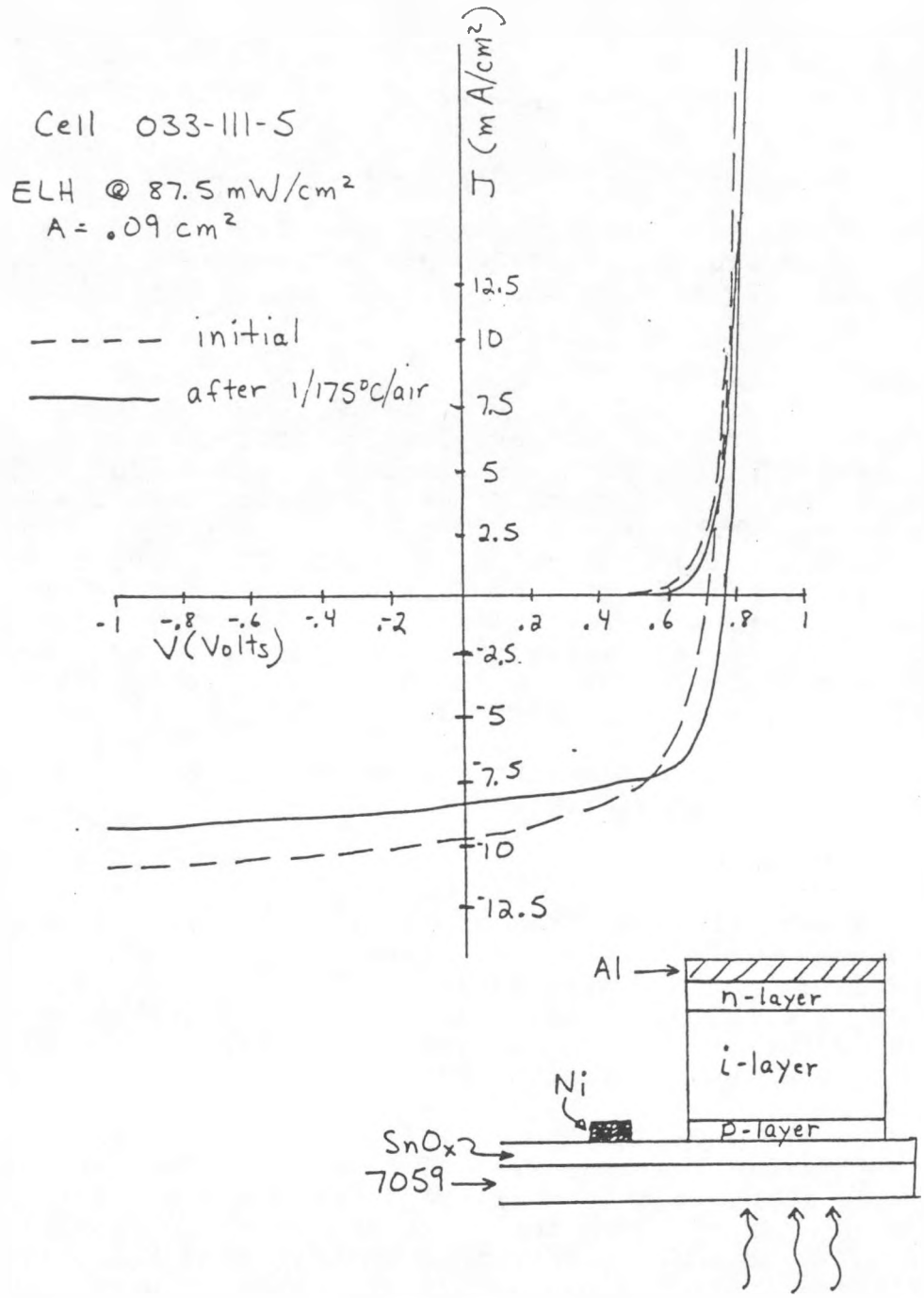

FIGURE 11. J-V Behavior of Cell 33.111-5 before and after Heat Treatment.

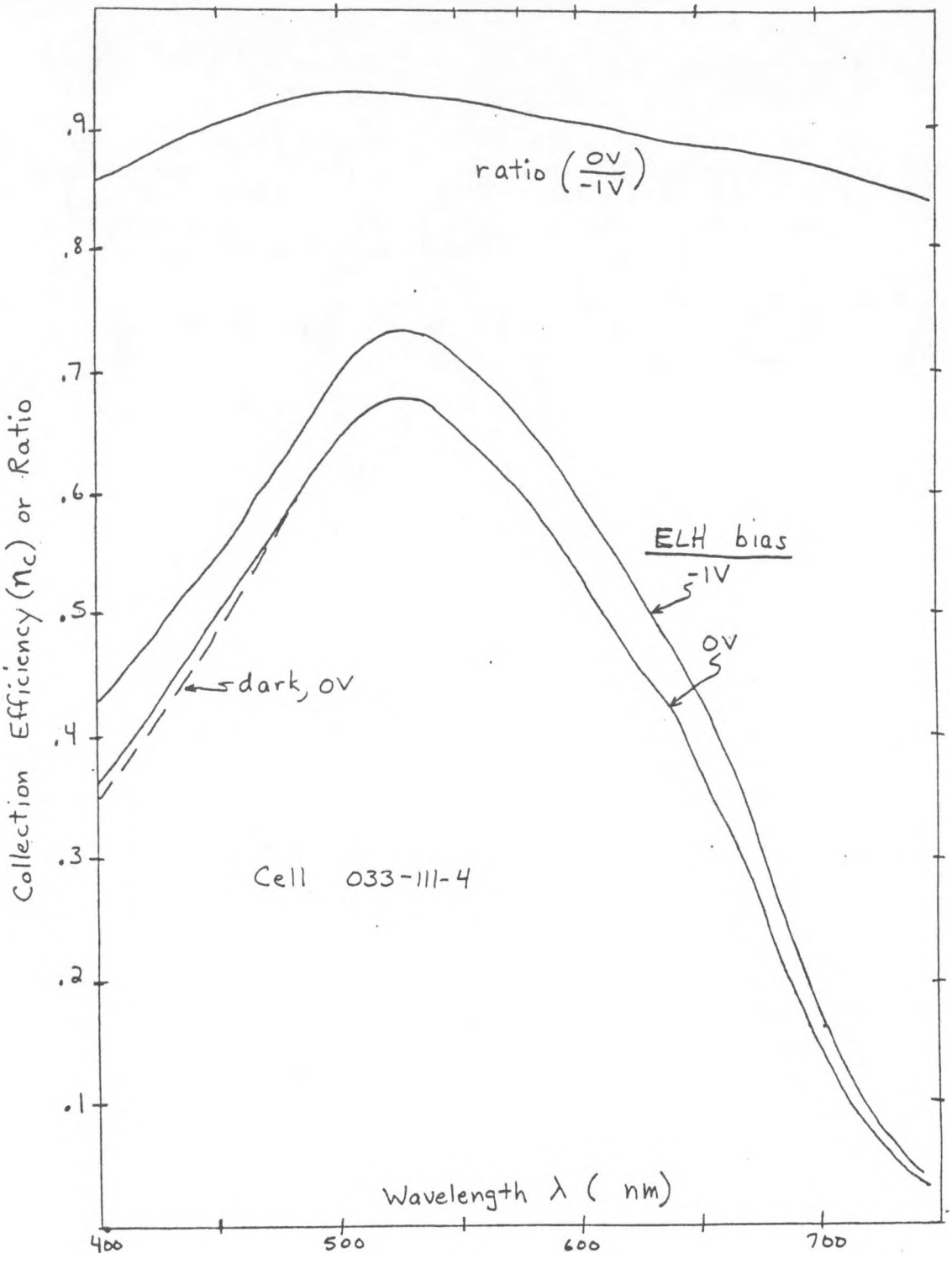

FIGURE 12. Collection Efficiency of Photo-CVD pin Cell with Voltage and Light Bias

with and without light bias indicates that space charge trapping modification of the field profile is negligible.

The reduced blue response is due to electrical losses, as indicated by the improvement in blue response with reverse bias, and to optical losses, as indicated by the rather low value which resulted even with reverse bias. The long wavelength response in Figure 11 is limited primarily by insufficient absorption due to the thin i-layer.

These results, particularly the values of diode factor and the low series resistance give encouragement that high efficiency devices can be made from photo-CVD deposited layers. Increased efficiency will result from implementing well-known a-Si device design features, such as a wide-gap front contact; reflective back contact; thicker i-layers; improved doped layers; and improved process control during transitions.

SECTION 4.0

APPENDIX A

Summary of Cell Test Results

Photo CVD Devices
9 January 1986

Test Date	Voc (V)	Jsc (mA/cm^2)	FF (%)	Eff (%)	HeatTreat. Hr/Deg/Atm	Test Comm
			Piece # PCV033.111 Cell # 1			
30-Oct-85	.663	10.15	59.80	4.60		GOOD
5-Nov-85	.666	9.85	60.15	4.51		GOOD
5-Nov-85	.404	8.82	30.20	1.23	1.00/175/AIR	UNSTA
			Piece # PCV033.111 Cell # 2			
30-Oct-85	.679	9.94	58.87	4.54		GOOD
5-Nov-85	.684	9.65	59.16	4.47		GOOD
5-Nov-85	.738	8.71	65.42	4.81	1.00/175/AIR	GOOD
			Piece # PCV033.111 Cell # 3			
30-Oct-85	.681	9.94	57.65	4.46		GOOD
			Piece # PCV033.111 Cell # 4			
30-Oct-85	.690	10.24	57.35	4.63		GOOD
5-Nov-85	.684	9.94	57.47	4.47		UNSTA
5-Nov-85	.746	8.92	65.42	4.98	1.00/175/AIR	GOOD

Test Date	Voc (V)	Jsc (mA/cm^2)	FF (%)	Eff (%)	HeatTreat. Hr/Deg/Atm	Test Comm
			Piece # PCV033.111 Cell # 5			
30-Oct-85	.707	9.92	57.18	4.59		GOOD
5-Nov-85	.706	9.66	56.80	4.43		GOOD
5-Nov-85	.766	8.53	65.22	4.87	1.00/175/AIR	GOOD
18-Dec-85	.765	9.08	64.61	5.13		GOOD
18-Dec-85	.749	6.02	65.00	5.08		GOOD
18-Dec-85	.729	3.72	65.04	4.98		GOOD
18-Dec-85	.713	2.58	65.35	5.54		GOOD
18-Dec-85	.694	1.69	65.79	5.40		GOOD
18-Dec-85	.671	0.93	66.17	4.70	Reduced Light Intensity	GOOD
18-Dec-85	.652	0.61	66.38	4.54		GOOD
18-Dec-85	.633	0.37	66.38	4.34		GOOD
18-Dec-85	.618	0.26	66.54	4.76		GOOD
18-Dec-85	.599	0.17	66.30	4.76		GOOD
18-Dec-85	.576	0.10	67.03	3.99		GOOD
			Piece # PCV033.111 Cell # 6			
30-Oct-85	.710	9.90	57.19	4.60		GOOD
5-Nov-85	.714	9.63	57.37	4.51		GOOD
5-Nov-85	.770	8.44	65.36	4.85	1.00/175/AIR	GOOD
			Piece # PCV033.111 Cell # 7			
30-Oct-85	.661	10.12	48.81	3.73		GOOD
5-Nov-85	.581	9.84	35.66	2.33		GOOD
			Piece # PCV033.111 Cell # 8			
30-Oct-85	.717	9.84	57.18	4.62		GOOD
5-Nov-85	.720	9.56	57.15	4.50		GOOD
5-Nov-85	.775	8.18	65.63	4.76	1.00/175/AIR	GOOD

Test Date	Voc (V)	Jsc (mA/cm^2)	FF (%)	Eff (%)	HeatTreat. Hr/Deg/Atm	Test Comm
			Piece # PCV033.111 Cell # 9			
30-Oct-85	.720	9.66	57.11	4.54		GOOD
5-Nov-85	.660	9.28	32.52	2.28		UNSTA
5-Nov-85	.767	8.01	54.51	3.83	1.00/175/AIR	UNSTA
			Piece # PCV033.111 Cell # 10			
30-Oct-85	.690	9.94	58.35	4.58		GOOD
			Piece # PCV033.111 Cell # 11			
30-Oct-85	.708	9.67	57.33	4.49		GOOD
			Piece # PCV033.111 Cell # 12			
30-Oct-85	.711	9.47	56.93	4.38		GOOD
5-Nov-85	.711	9.13	58.04	4.31		GOOD
5-Nov-85	.771	7.74	65.51	4.47	1.00/175/AIR	GOOD

REFERENCES

1. R. E. Rocheleau et al. in Materials Issues in Applications of Amorphous Silicon Technology. MRS Symposia Proceedings Vol. 49. pp 15-20.

   B. N. Baron, et al., "Chemical Vapor Deposition of Amorphous Semiconductor Films", SERI/STR-211-2711, Golden, CO, Solar Energy Research Institute (1985).

2. Y. Mishima et al. Japan J. Appl. Phys. 22, L46(1983).

3. T. Saitoh et al., Appl. Phys. Lett. 42(8), 678(1983).

4. T. Inoue et al., Appl. Phys. Lett 43(8), 774(1983).

5. A. E. Delahoy et al. in Materials Issues in Applications of Amorphous Silicon Technology. MRS Symposia Proceedings Vol. 49. pp 33.

6. M. Konagai et al. Proc. 18th IEEE Photovoltaic Spec. Conf. Las Vegas, Oct 1985. To be published.

7. T. Kazahaya et al. Technical Digest of the International PVSEC-1, Koba, Japan(1984) p. 449.

8. D. D. Allred et al., U.S. Patent No. 4,435,445.

9. J. W. Peters and F. L. Gebhart U.S. Patent No. 4,265,932.

10. M. H. Brodsky et al. Phys. Rev. B. 16(8), 3556(1977).

11. W. denBoer, J. Physique 4,451(1981).

12. G. A. Swartz, in Semiconductors and Semimetals 21D, ed J. Pankove, Academic Press, 39(1984).